

## Article

# Exploring Spatio-Temporal Precipitation Variations in Istanbul: Trends and Patterns from Five Stations across Two Continents

Yiğitalp Kara <sup>1,2</sup>, Veli Yavuz <sup>1</sup>, Caner Temiz <sup>2</sup> and Anthony R. Lupo <sup>3,\*</sup>

<sup>1</sup> Department of Meteorological Engineering, University of Samsun, 19 Mayıs, 55000 Samsun, Türkiye; yigitalp.kara@samsun.edu.tr (Y.K.); veli.yavuz@samsun.edu.tr (V.Y.)

<sup>2</sup> Department of Meteorological Engineering, Istanbul Technical University, Ayazaga, 34469 Istanbul, Türkiye; temizc@itu.edu.tr

<sup>3</sup> Atmospheric Science Program, University of Missouri, 302 E ABNR, Columbia, MO 65211, USA

\* Correspondence: lupoa@missouri.edu

**Abstract:** This study aims to reveal the long-term station-based characteristics of precipitation in Istanbul, a mega city located on the continents of Europe and Asia, with complex topography and coastline along the Marmara and Black Seas. Using data from five different stations, three located in the European continent and two in the Asian continent, with measurement periods ranging from 72 to 93 years, wet and dry days have been identified, statistics on precipitation conditions during the warm and cold seasons have been generated, categorization based on precipitation intensities has been performed, and analyses have been conducted using extreme precipitation indices. At stations located in the northern part of the city, higher annual total precipitation has been observed compared to those in the south. A similar situation applies to the number of wet days. While during the cold season, the wet and dry day counts are nearly the same across all stations, this condition exhibits significant differences in favor of dry days during the warm season. Apart from dry conditions, “moderate” precipitation is the most frequently observed type across all stations. However, “extreme” events occur significantly more often (6%) during the warm season compared to the cold season (2%). Long-term anomalies in terms of annual precipitation totals have shown similarity between stations in the north and south, which has also been observed in longitudinally close stations. Despite the longer duration of the cold season and stronger temperature gradients, extreme rainfall events are more frequent during the warm season, primarily due to thunderstorm activity. While trend analyses revealed limited significant trends in precipitation intensity categories and extreme indices, the study highlights the importance of comprehensive examination of extreme rainfall events on both station-based and regional levels, shedding light on potential implications for regional climate change. Lastly, during the cold season, the inter-station correlation in terms of annual total precipitation amounts has been considerably higher compared to the warm season.

**Keywords:** precipitation intensity; rainfall; extreme climate indices; cold season; warm season



**Citation:** Kara, Y.; Yavuz, V.; Temiz, C.; Lupo, A.R. Exploring Spatio-Temporal Precipitation Variations in Istanbul: Trends and Patterns from Five Stations across Two Continents. *Atmosphere* **2024**, *15*, 539. <https://doi.org/10.3390/atmos15050539>

Academic Editor: Tomeu Rigo

Received: 26 March 2024

Revised: 18 April 2024

Accepted: 24 April 2024

Published: 28 April 2024



**Copyright:** © 2024 by the authors. Licensee MDPI, Basel, Switzerland. This article is an open access article distributed under the terms and conditions of the Creative Commons Attribution (CC BY) license (<https://creativecommons.org/licenses/by/4.0/>).

## 1. Introduction

Precipitation is a crucial component of the Earth’s water cycle, playing a vital role in sustaining natural ecosystems and informing human activities such as agriculture, energy production, and water supply [1,2]. The intensity of precipitation and drought are significant determinants of climate conditions, affecting natural ecosystems and human activities [3]. The intensity of precipitation determines the quantity and distribution of water sources in geographic regions. Heavy rainfall can increase the risk of flooding, cause soil erosion, and put pressure on water resources. On the other hand, low precipitation levels and drought can lead to serious problems in agriculture, water resource management, energy production, and other sectors [4–11]. Therefore, the analysis of long-term precipitation data is of critical importance for making informed decisions in areas such as climate change, water management, and strategies for coping with natural disasters [12,13].

There are numerous studies worldwide that examine trend analyses of precipitation amounts and intensity. Some key findings from these studies include the following: In the case of South China, a noticeable drought trend has been observed due to rising temperatures [14]. Studies conducted for Central Asia have revealed a relationship between changes in precipitation frequency and precipitation concentrations [10]. In research focused on Pakistan, it has been reported that drought periods can extend up to 10 months [15]. For Bangladesh, an increase in the frequency index of rainy days has been noted, accompanied by a significant decrease in precipitation intensity indices [16], and different trends have been detected in various precipitation categories [17]. In Ethiopia, an overall decreasing trend in annual total precipitation has been identified [18]. In Kenya, a decreasing trend in annual rainfall has been observed, with different regions showing varying trends seasonally [19]. The general conclusion drawn from studies conducted in different continents and countries worldwide reveals trends such as a decrease in the frequency of rainy periods on an annual basis, an increase in the frequency of intense and heavy rainfall, varying trends in both the frequency and intensity of rainy days seasonally, and an increase in trends related to dry conditions and dry days.

Global climate change, regional climate variations, and the associated global warming are expected to result in changes in the amount, intensity, frequency, and duration of precipitation [9]. Analyses using long-term climatological datasets and model simulations indicate an increasing trend in extreme rainfall both regionally and globally [20–22]. Numerous studies utilize long-term rain gauge data, reanalysis datasets, satellite precipitation products, etc., to calculate extreme climate indices, revealing regional trends [23,24]. Guo et al. (2020) calculated concentration-index and precipitation concentration-index values using data from multiple stations across mainland China and conducted trend tests, determining return periods for dry periods based on this information [25]. Wu and Chen (2019) calculated the intensity of dry periods over the years using drought indices with data from 42 meteorological stations [14]. Rahman et al. (2019) examined precipitation intensities for Bangladesh using numerous precipitation intensity indices and data from 23 stations [16]. Mahmoud et al. (2019) conducted long-term analyses using satellite data and ground observation data for the United Arab Emirates [26]. Mumo et al. (2019) and Pawar et al. (2023) performed analyses of long-term precipitation data using various nonparametric trend tests, statistically examining the annual and intra-year variations in precipitation [19,27]. Anderson et al. (2019) detected changes in precipitation for Central America by conducting multiscale trend analyses for rainfall extremes [28]. Xiong et al., 2019, Bhatti et al., 2020, and Rao et al. (2020) conducted long-term analyses for each of the extreme climate rainfall indices, including annual precipitation totals, extreme rainfall analysis, and analyses of wet and dry days [29–31].

Numerous studies related to precipitation in Türkiye are present in the literature. In these studies, both cold-season precipitation [32–39] and warm-season precipitation [40–42] have been comprehensively addressed from dynamic and synoptic perspectives. Through various case analyses and long-term observations, studies have consistently highlighted an evident increase in intensity and frequency, particularly in both warm- and cold-season precipitation since the 21st century. Besides these mentioned studies, there are numerous other studies in the literature specifically conducted for Türkiye, addressing various aspects such as precipitation amounts, frequencies of wet–dry days, extreme precipitation indices, and precipitation intensities. In these studies, long-term annual trend analyses of rainy periods and total precipitation have been conducted [43–46], and monthly and/or seasonal precipitation regimes have been examined [47,48]. Long-term analyses of wet and dry season precipitations have been performed [49], and changes in precipitation intensity have been investigated on an annual basis [50].

In most of the studies in the literature, a decrease in the number of wet days has been observed on an annual basis in the southern regions of Turkey, while a significant trend has not been identified in the northern regions. Similarly, a general decrease in the total precipitation amounts has been observed, albeit the trends are limited. Regionally, a

limited increase in the frequency of extreme rainfall events has been detected, especially in the Mediterranean region [43,44,46–48]. Cluster analysis based on precipitation intensities has been conducted [51], and hydro-climatological analyses using satellite products and/or drought indices have been conducted [52,53]. Extreme rainfall events have been analyzed [54], and standard durations of maximum precipitation have been identified [55]. Performance analyses have been conducted by comparing satellite products and ground observation data [56]. Although all these studies include long-term analyses of rainy and rainless periods, trend analyses of extreme climate indices, long-term analyses of changes in total precipitation regimes, and analyses of precipitation intensities, none of them have conducted an analysis specifically focusing on precipitation in the warm and cold seasons. Furthermore, no study has been found that combines precipitation intensity categories with extreme climate indices in a comprehensive analysis with long-term trend assessments.

Of the surveyed stations, three are located on the European continent, and the remaining two are positioned on the Asian continent. Each continent is represented by a station along Istanbul's Black Sea coastline (Kilyos Station—European Continent; Sile Station—Asian Continent) and another station along the southern coast facing the Marmara Sea (Florya Station—European Continent; Kadikoy Station—Asian Continent). Additionally, a station near the midpoint of the Bosphorus, connecting the diverse climatic features of both continents, was included in the selection. This strategic station placement aims to capture the varied climatic influences of the Black Sea and the Marmara Sea, as well as the unique topographical characteristics of Istanbul's European and Asian regions.

In this study, long-term precipitation analyses have been conducted for the mega-city Istanbul using five different rain gauge datasets located on two different continents from 1929 to 2022 (data provided from the oldest station starts from 1929, while others vary). Starting with daily total precipitation datasets, the statistics of wet and dry days have been initially presented on an annual basis. Subsequently, precipitation intensity analyses have been conducted by categorizing precipitation into five different levels (trace, light, moderate, heavy, and extreme). Eight extreme precipitation indices have been employed to reveal long-term trends. In the second phase of the study, a detailed analysis of precipitation for the first time has been conducted specifically for the warm and cold seasons in Türkiye. In this context, Section 2.1 provides detailed information about the study area, long-term climatology of the city, and specific details about the five different stations from which data were obtained. Section 2.2 describes the methods employed in the study. In Section 3, all the results obtained in the study are explained in detail. Section 4 highlights important points from the study, and in Section 5, the study results are mutually analyzed in comparison with similar studies in the literature, emphasizing commonalities and differences.

## 2. Materials and Methods

### 2.1. Study Area and Data

Istanbul, a mega city bridging the continents of Asia and Europe, experiences a climate in transition between the Black Sea and the Mediterranean. According to the DeMartonne Climate Classification, based on the drought index, the city is categorized as semi-arid to moist (Drought index = 18.08). The Erinc Climate Classification, relying on the precipitation effectiveness index, and the Thornthwaite Climate Classification both classify it as humid to semi-humid. According to the Trewartha Climate Classification, which is based on the universal temperature scale, Istanbul has warm summers and cool winters. The Koppen Climate Classification characterizes it as a climate with warm winters and very hot and dry summers (Mediterranean climate). As per the Koppen–Trewartha Climate Classification, it exhibits a subtropical dry summer climate and a Mediterranean climate [57]. Analyzing meteorological station measurements spanning from 1929 to 2022, it is observed that the city experienced its highest daily total precipitation in September 1981, reaching 136.1 mm. The most intense daily wind speed, recorded at 20.8 m/s, occurred in October 2010. Over the measurement period, the highest temperature, reaching 40.6 °C, occurred in July, whereas the lowest temperature, −9 °C, was recorded in February.

For the purpose of this study, an examination was conducted at five meteorological stations where the lengthiest measurements in the city were taken. The analysis was performed utilizing synoptic observations published by meteorological stations in the study. Although daily total precipitation data were obtained for different periods for all stations, even the most recent one has a dataset spanning 72 years from 1951 to 2022. Among these stations, three are positioned on the European continent, while the remaining two are situated on the Asian continent. Furthermore, one station from each continent was selected at points along the city's Black Sea coastline (Kilyos Station—European Continent; Sile Station—Asian Continent). Additionally, one station was chosen from points along the southern coast facing the Marmara Sea, on both the European and Asian continents (Florya Station—European Continent; Kadikoy Station—Asian Continent). Another station was selected from a location near the middle of the Bosphorus, connecting the two continents. The station selections aimed to observe the distinct effects of both the Black Sea and the Marmara Sea, as well as the Bosphorus individually (Figure 1). Detailed information about the stations is provided in Table 1.

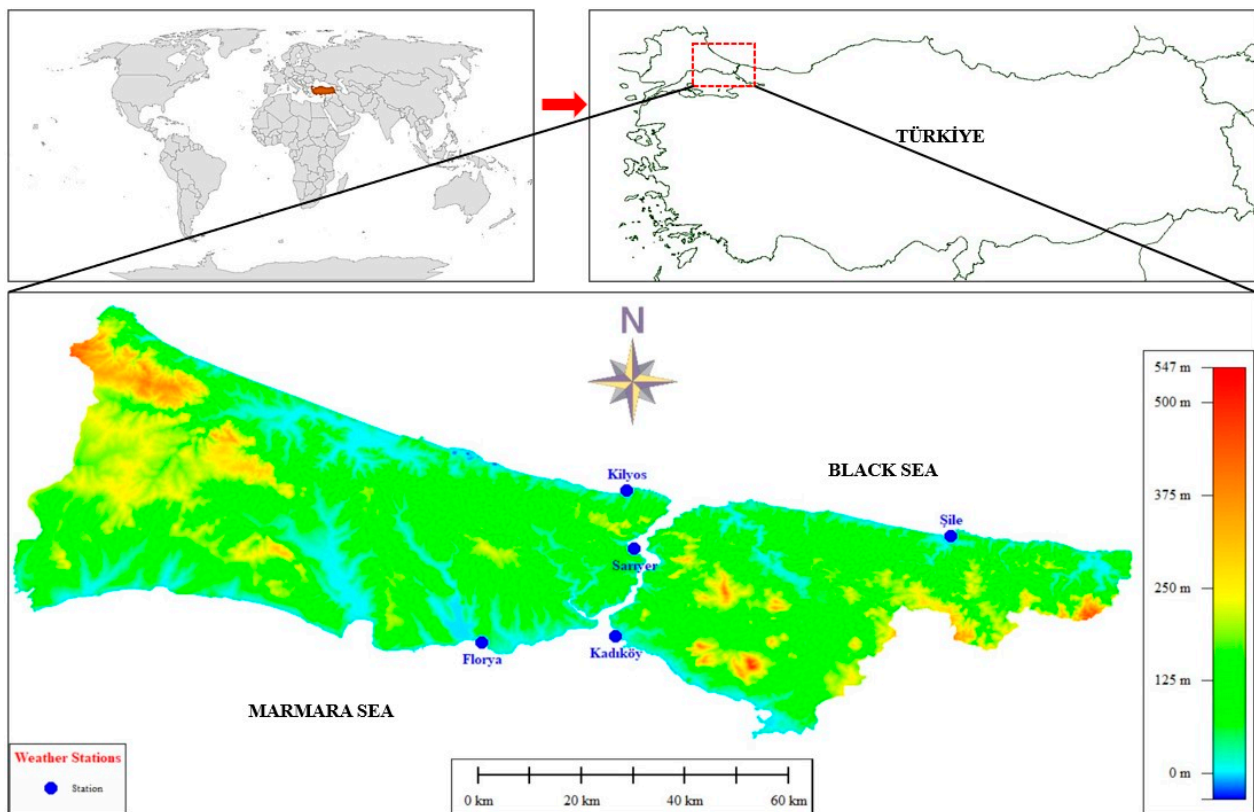


**Figure 1.** Study area and locations of the meteorological stations.

**Table 1.** Detailed information on meteorological stations [58].

Stations	WMO Station ID	Latitude	Longitude	Altitude	Period
Florya	17636	40.9758°	28.7865°	37.0 m	1937–2022
Kadikoy	17062	40.9883°	29.0190°	5.0 m	1929–2022
Kilyos	17059	41.2505°	29.0384°	38.0 m	1951–2022
Sariyer	17061	41.1464°	29.0502°	59.0 m	1949–2022
Sile	17610	41.1688°	29.6007°	83.0 m	1940–2022

## 2.2. Methodology

In the study, initially wet and dry days were identified, followed by cold and warm seasons (Section 2.2.1). Subsequently, precipitation intensity categories were established based on the amount of precipitation (Section 2.2.2). The trend tests to be applied later were determined, which will be used both in precipitation intensity categories and extreme precipitation indices (Section 2.2.3). Finally, the selection of which extreme precipitation indices would be utilized in the study and their definitions were established (Section 2.2.4).

### 2.2.1. The Determination of Dry/Wet Days and Warm/Cold Seasons

Dry days are characterized by daily total precipitation amounts less than 0.1 mm, while wet days refer to periods when the daily total precipitation is 0.1 mm or more [59]. In this study, a threshold of 0.1 mm has been employed to classify wet and dry days.

In analyses related to atmospheric events and meteorological variables, in some cases, the terms warm and cold seasons are used instead of normal seasons. The most significant reason for this is the changes in the durations, start, and end times of classical seasons under the influence of regional/global climate change. In this context, the warm season is used to represent the period between May and September, while the cold season is used to represent the period between October and April. The warm season consists of a total of 5 months, whereas the cold season consists of a total of 7 months [60]. In this study, a similar approach to the literature is adopted for the warm and cold seasons.

### 2.2.2. The Creation of Precipitation Intensity Categories

For a specific location, daily precipitation distributions can be characterized by examining values in the lower and upper tails [61]. For very intense and extreme precipitation events, the upper tail is often preferred as >90th percentile [62,63]. In some studies, classifications are made based on specific threshold values. For example, Ma et al. (2015) used the following categories: “trace” for precipitation amounts less than 0.1 mm/day, “light” for amounts between 0.1 and 10 mm/day, “moderate” for amounts between 10 and 25 mm/day, “heavy” for amounts between 25 and 50 mm/day, and “very heavy” for amounts  $\geq 50$  mm/day [64].

In this study, boxplots were created for stations to depict precipitation amounts below <25th percentile, between 25th and 75th percentiles, between 75th and 90th percentiles, and above >90th percentile. Subsequently, the terms “trace” were used for days with precipitation amounts less than 0.1 mm, “light” for days when it was <25th percentile, “moderate” for days between 25th and 75th percentiles, “heavy” for days between 75th and 90th percentiles, and “extreme” for days > 90th percentile.

### 2.2.3. Trend Analysis

The Mann–Kendall (MK) trend test is commonly employed for detecting significant trends within long datasets [65,66]. Sen’s Slope Estimator (SS), on the other hand, is utilized in the long-term analysis of meteorological variables to reveal trends and estimate the magnitude of the slope [67]. The Mann–Kendall trend test, conducted based on the ranks of the data, is unaffected by the data distribution and less sensitive to outliers. In contrast, parametric trend tests, although more powerful, require normal distribution in the data and are more sensitive to outliers. Therefore, the Mann–Kendall test and other non-parametric trend tests may be more suitable for detecting trends in hydrological time series, which often involve skewed and outlier-laden data [68–70].

Mann–Kendall test statistic “S” is calculated for a given time series  $X = \{x_1, x_2, x_3, \dots, x_n\}$  as follows:

$$S = \sum_{i=1}^{n-1} \cdot \sum_{j=i+1}^n \text{sign}(x_j - x_i) \tag{1}$$

$$\text{sign}(x_j - x_i) = \begin{cases} +1, & (x_j - x_i) > 0 \\ 0, & (x_j - x_i) = 0 \\ -1, & (x_j - x_i) < 0 \end{cases} \tag{2}$$

where  $n$  is the sample size,  $x_i$  and  $x_j$  represent the data values in times series  $i$  and  $j$  ( $j > i$ ), and  $\text{sign}(x_j - x_i)$  represent the sign function.

The variance value is calculated as follows:

$$\text{Var}(S) = \frac{n(n-1)(2n+5) - \sum_{i=1}^m t_i(t_i-1)(2t_i+5)}{18} \tag{3}$$

where  $m$  represents the number of tied groups and  $t_i$  denotes the number of pairs of tied values. When the sample size  $n > 10$ , the  $Z$ -test statistics is calculated as follows:

$$Z = \frac{S \pm 1}{\text{Var}(S)^{1/2}} \tag{4}$$

Positive  $Z$  values indicate an upward trend, while negative values indicate a downward trend. Testing trends are conducted for a specific significance level “ $\alpha$ ”. This value is typically set to 0.01 or 0.05.

Sen’s Slope offers an advantage over linear regression as it is not influenced by the presence of outliers and data errors. The Sen’s Slope equation for  $N$  data sample pairs is expressed as follows:

$$Q_i = \frac{(x_j - x_i)}{j - i}, i = 1, 2, 3, \dots, N \tag{5}$$

where  $x_j$  and  $x_i$  represent data values at times  $j$  and  $i$  (where  $j > i$ , respectively). If there are  $N$  values of  $x_j$  in the time series, the number of slope estimates  $N$  will be calculated as  $N = n(n-1)/2$ . The  $Q_i$  values, totaling  $N$  are sorted in ascending order, and Sen’s Slope is based on the median  $Q_i$  ( $Q_{med}$ ). A two-tailed test evaluates the value of  $Q_{med}$  within the confidence intervals 90% and 95%, computed as follows:

$$Q_{med} = \begin{cases} Q_{[\frac{N+1}{2}]} & \text{if } N = \text{odd} \\ Q_{[\frac{N}{2}]} + Q_{[\frac{N+1}{2}]} & \text{if } N = \text{even} \end{cases} \tag{6}$$

#### 2.2.4. Extreme Precipitation Indices

In this study, eight precipitation indices from the extreme climate indices prepared by the Expert Group on Climate Change Detection and Indices (ETCCDI) were analyzed [71] Detailed information regarding these indices is provided below.

**PRCPTOT:** Annual cumulative precipitation on days with recorded rainfall

Consider  $RR_{ij}$  as the daily precipitation amount on Day  $i$  in Period  $j$ .

$$\text{PRCPTOT}_j = \sum_{i=1}^I RR_{ij} \tag{7}$$

**Rx1day:** Maximum 1-day precipitation

Consider  $RR_{ij}$  as the daily precipitation amount on Day  $i$  in Period  $j$ . The maximum 1-day value for Period  $j$  is denoted as  $Rx1day_j$  and is determined by the maximum value among all  $RR_{ij}$  values.

**Rx5day:** Maximum 5-day precipitation

Consider  $RR_{kj}$  as the precipitation amount on for the 5-day interval ending on Day  $k$  in Period  $j$ . The maximum 5-day values for period  $j$  are denoted as  $Rx5day_j$  and are determined by finding the maximum value among all  $RR_{kj}$  values.

**R10mm:** Annual count of days when precipitation amount  $\geq 10$  mm

Consider  $RR_{ij}$  as the daily precipitation amount on Day  $i$  in Period  $j$ . Count the days where  $RR_{ij}$  is greater than or equal to 10 mm.

**R20mm:** Annual count of days when precipitation amount  $\geq 20$  mm

Consider  $RR_{ij}$  as the daily precipitation amount on Day  $i$  in Period  $j$ . Count the days where  $RR_{ij}$  is greater than or equal to 20 mm.

**R50mm:** Annual count of days when precipitation amount  $\geq 50$  mm

Consider  $RR_{ij}$  as the daily precipitation amount on day  $i$  in period  $j$ . Count the days where  $RR_{ij}$  is greater than or equal to 50 mm.

**CDD:** Consecutive Dry Days

Maximum duration of a dry spell: the highest count of consecutive days with precipitation less than 1 mm. Consider  $RR_{ij}$  as the daily precipitation amount on Day  $i$  in Period  $j$ . Determine the maximum count of consecutive days where  $RR_{ij}$  is lower than 1 mm.

**CWD:** Consecutive Wet Days

Maximum duration of a wet spell: the highest count of consecutive days with precipitation equal to or exceeding 1 mm. Consider  $RR_{ij}$  as the daily precipitation amount on Day  $i$  in Period  $j$ . Determine the maximum count of consecutive days where  $RR_{ij}$  is greater than or equal to 1 mm.

### 3. Annual Total Precipitation Amounts, Wet/Dry Day Statistics, and Warm/Cold Season Statistics

Information regarding annual total precipitation amounts since the inception of station operations for five different stations located in Istanbul (Florya, Kadikoy, Kilyos, Sariyer, and Sile) is provided in Figure 2. Florya has an annual average total precipitation of 648.1 mm over an 86-year period; for Kadikoy, it is 677.2 mm over a 94-year period; for Kilyos, it is 796.6 mm over a 72-year period; for Sariyer, it is 823.6 mm over a 73-year period; and for Sile, it is 818.5 mm over an 83-year period (Figure 2). The month exhibiting the highest total precipitation on a monthly basis (ranging from 97.2 to 122.5 mm) for all stations has been December. On the contrary, except for Kadikoy (where it occurs in December), the month with the highest number of rainy days for all other stations has been January (not shown). In the annual analysis conducted separately for each station, it is observed that in the Sile station, the precipitation in 1979 was nearly twice the average (Figure 3). This situation is thought to be due to Sile’s geographical location (on the coast of the Black Sea, in a mountainous region), resulting in short but intense rainfall exposure, with a high frequency of such events in that year. Overall, the higher annual total precipitation amounts in the three stations located in the north (Sile, Sariyer, and Kilyos) compared to the two stations in the south (Kadikoy and Florya) also confirm this.

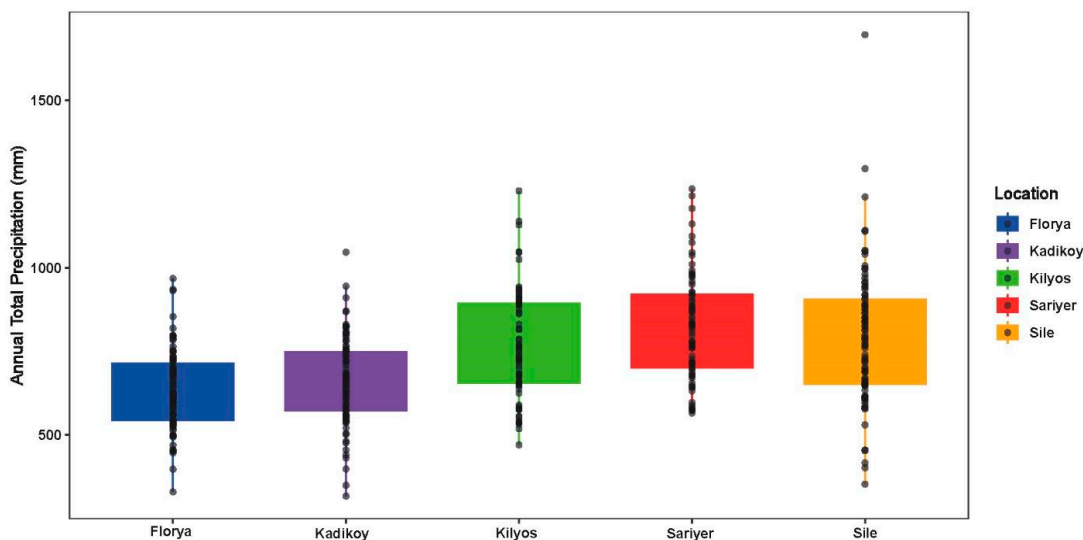


**Figure 2.** The long-term average annual total precipitation amounts (mm) for five different stations located in Istanbul.

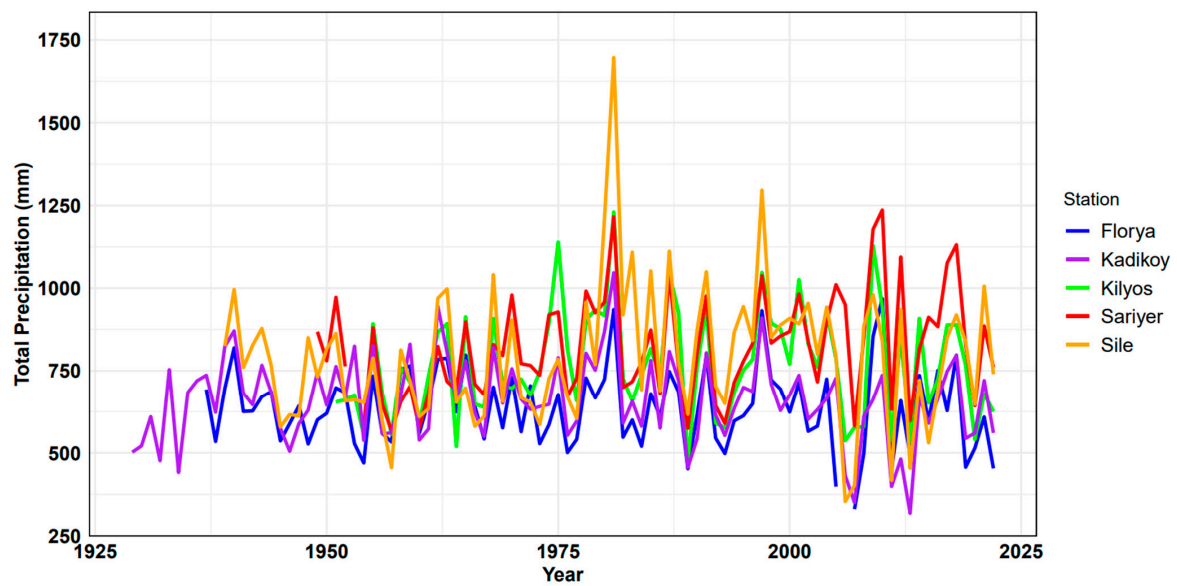


**Figure 3.** As in Figure 2, but on an annual basis.

In Figure 4, the frequencies of wet days' annual averages for each station within the specified periods are provided for five different stations. No trend analysis has been conducted in this graph, and detailed analyses will be performed in subsequent sections. The annual average frequencies of wet days have shown results entirely similar to the analysis results of annual total precipitation amounts. The highest frequency values have been observed in the three stations located in the northern part of the city, while lower frequencies have been identified in stations located in the southern part of the city. The annual average number of wet days is 128.64 days/year for Sariyer, 124.10 days/year for Kilyos, 112.70 days/year for Sile, 108.21 days/year for Florya, and 103.50 days/year for Kadikoy (Figure 4). Additionally, analyses conducted for monthly frequencies of wet days have revealed that the highest frequencies are observed in January in all stations (14.79–17.43 days/month). Furthermore, to understand the difference between wet days and rainy days, snowfall, hail, frost, and dew days have also been examined. Frequencies of hail, frost, and dew days were found to be quite low, while annual frequencies of snowfall days ranged from 9.64 days/year to 10.65 days/year.

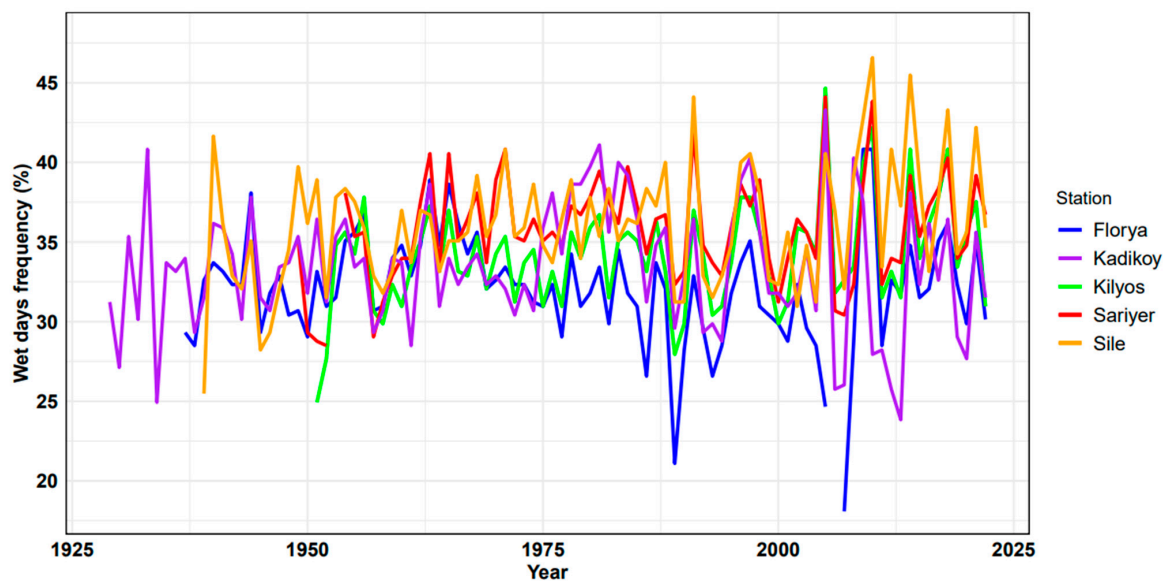


**Figure 4.** The separate annual average wet day frequencies for each station.

For all stations, separate frequency analyses of wet and dry days during the warm and cold seasons have been conducted (Figure 5). The frequency of wet days during the cold season is at least twice as high as during the warm season. Station-wise, the frequencies of wet days during the cold season ranged from 42% to 51%, while during the warm season, these ratios were in the range of 17% to 22%. Therefore, it is crucial to first understand the behavior during the cold season for the analysis of rainy days, both in the northern and southern parts of the city. In their study analyzing synoptic weather types for the Marmara Region, including Istanbul, Baltaci et al. (2012) revealed the influence of six significant synoptic weather types on the region and their frequencies. According to these findings, the dominant synoptic weather types in the region are: 24% northeast, 21% north, 11% south, 9% southwest, 7% anticyclonic, and 5% cyclonic [72]. As evident from these results, northerly flows prevail throughout the region. Although these ratios vary between the warm and cold seasons, it is a fact that, particularly in stations located in the northern part of Istanbul, air masses receiving moisture from the Black Sea bring more rainfall to the city. This situation has also been expressed in a study by Baltaci et al. (2017), stating that especially northeastern flows lead to the maximum daily rainfall potential in the region [73].

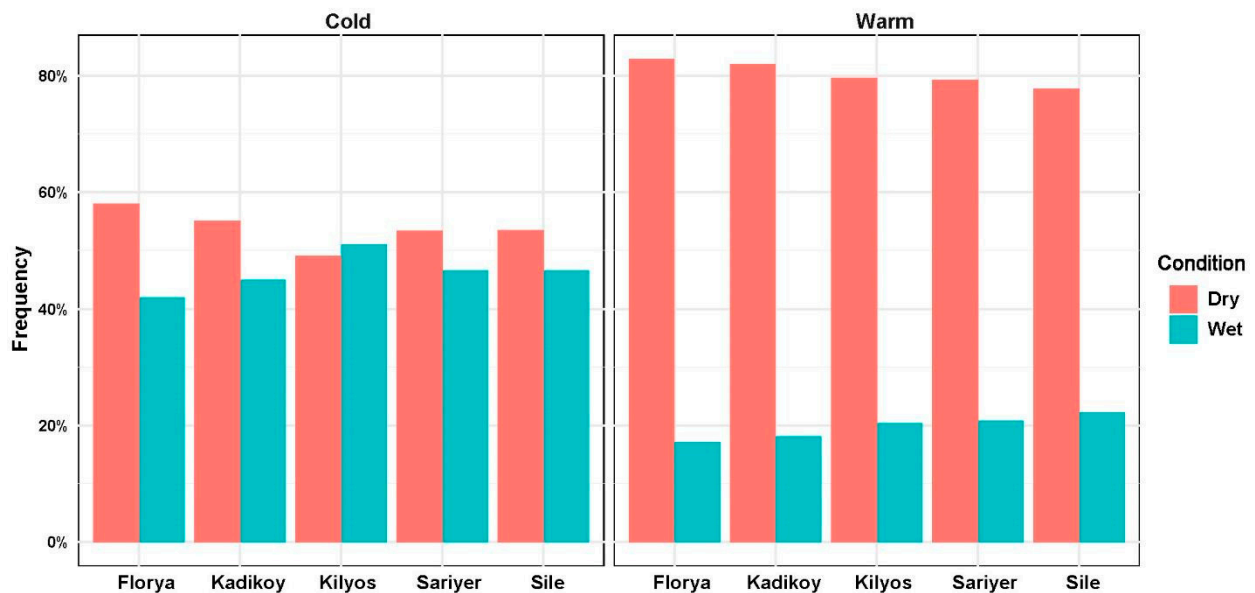


**Figure 5.** The wet- and dry-day frequencies for the stations during cold and warm seasons.

#### 4. Analysis of Station-Based Rainfall Intensity Categories

In the previous section, analyses were conducted regarding annual total precipitation amounts and wet- and dry-day frequencies during the warm and cold seasons for five different stations located in various regions across Istanbul. In this section, detailed analyses were carried out on a station-by-station basis to determine the distribution of precipitation intensities throughout the city. The aim of these analyses is to identify trends in precipitation intensities for each station during both warm and cold seasons, and to determine the differences between stations. Accordingly, using the method outlined in Section 2.2.2, analyses were conducted on a station-by-station basis in five different categories based on precipitation amounts. First, frequencies of precipitation intensities were determined based on annual total precipitation amounts for each station (Figure 6a), followed by similar analyses for cold (Figure 6b) and warm seasons (Figure 6c). In the analyses conducted on an annual basis, no significant difference was observed among stations in terms of precipitation intensity categories. The highest frequency occurred in the “trace” category, followed by “moderate” and “light” categories, respectively, across all stations. On the other hand, the lowest frequencies occurred in the “extreme” category across all stations (Figure 6a). In the cold season, there is almost no difference in frequency among stations for extreme precipitation events; however, this is not the case in the warm season. In the warm

season, the “extreme” category at the Sile station has a slightly higher frequency compared to other stations (Figure 6b,c). This phenomenon can be explained by the station’s coastal location on the Black Sea, where it is exposed to convective cell structures due to northerly flows. Similar conditions apply to the Kilyos station as well. In both cold and warm seasons, the “moderate” category has the highest frequency at the Sile station, followed by the Sariyer station (Figure 6b,c). In the cold season, the frequency of the “moderate” category is above 20% across all stations (Figure 6b), whereas this ratio drops to the 10% range in the warm season (Figure 6c). Similar patterns are observed in other categories as well (Figure 6b,c).

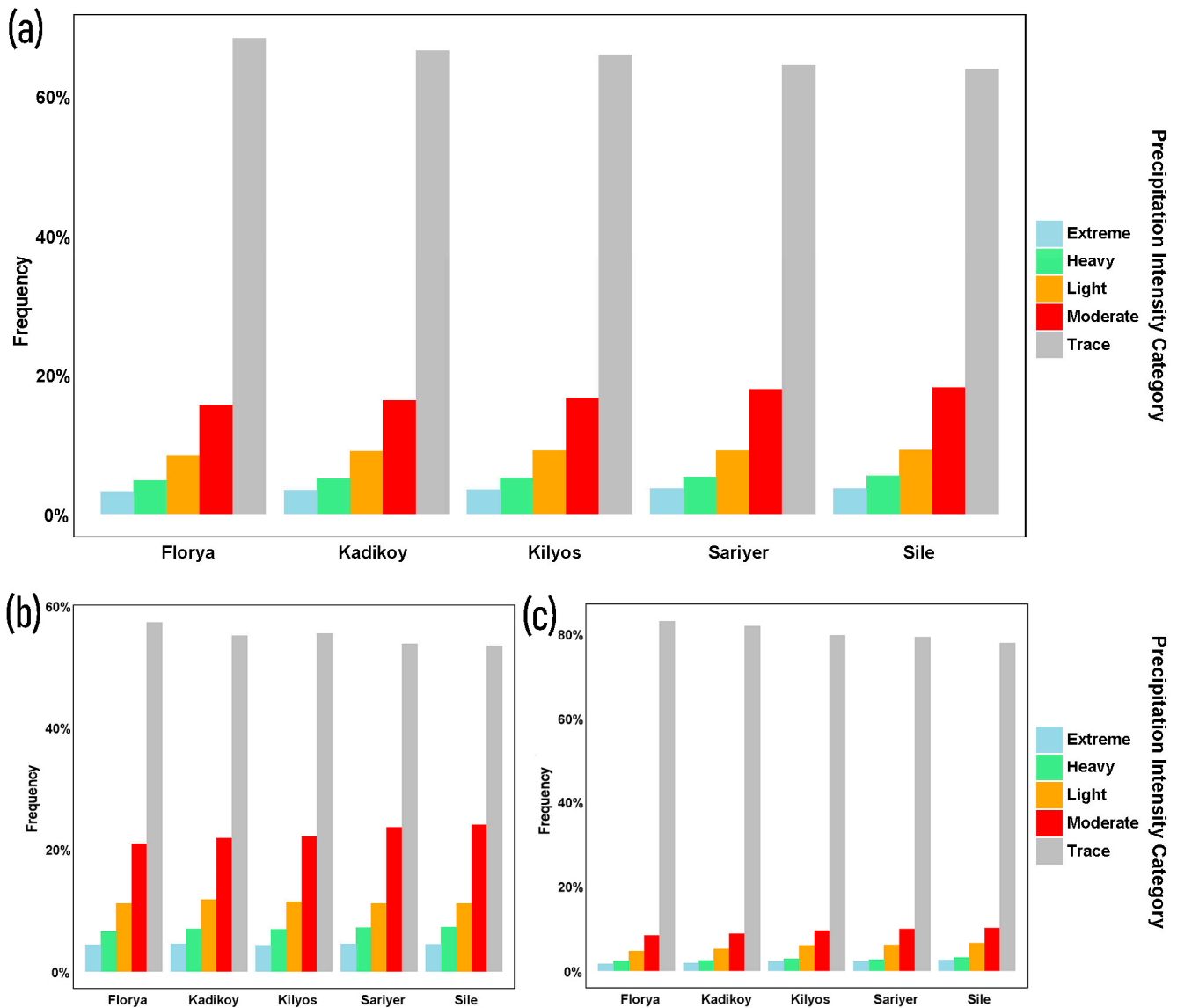


**Figure 6.** The frequencies of (a) annual, (b) warm-season, and (c) cold-season precipitation intensity categories for each station.

### 5. Annual Station-Based Rainfall Total Anomalies

In this section, annual precipitation total anomalies for each station have been examined. The changes exhibited by stations on an annual basis have varied. The most variable anomaly values were observed at the Sile station. Negative anomaly values were observed at this station from the beginning of the period until 1975, while positive anomaly values were more frequently observed between 1975 and 2005. However, mostly negative anomalies are observed between 2005 and 2022. On the other hand, other stations do not

exhibit sharp distinctions as the Sile station. Negative anomalies have been predominantly observed at the Kadikoy station since the early 2000s, while at the Sariyer station, positive anomalies have been observed. Evaluating the northern and southern stations of the city, similar anomaly trends have been found at the Kadikoy and Florya stations located in the south. However, such a trend is not evident at the Sile and Kilyos stations located in the north of the city. The main reason for this is the greater distance between northern stations compared to southern stations. Indeed, there is a similar trend between the Kilyos and Sariyer stations, just like between the Sile and Kilyos stations (Figure 7).

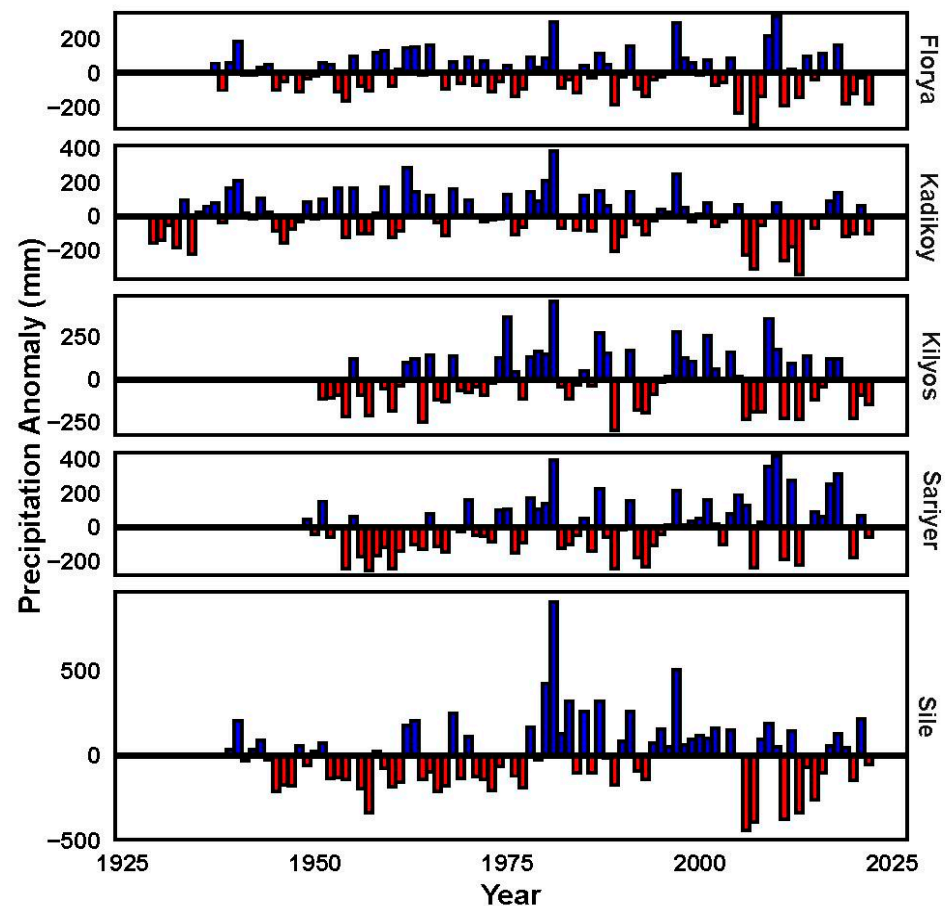
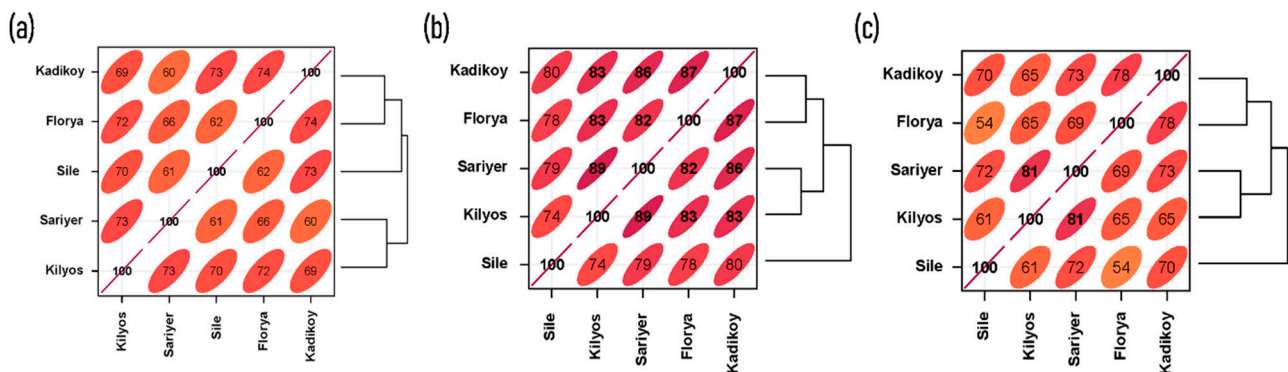


Figure 7. The individual-based anomaly values of annual precipitation totals for the stations.

## 6. Inter-Station Correlations of Annual, Warm-Season, and Cold-Season Total Precipitation

In this section, inter-station correlations were analyzed using the total precipitation datasets of the stations. Accordingly, the Pearson Correlation was used to prepare correlation matrices and dendrograms for the annual (Figure 8a), warm-season (Figure 8b), and cold-season categories (Figure 8c). The highest correlation between stations on an annual basis (0.74) was found between Kadikoy and Florya stations. This was followed by the correlations between Kilyos and Sariyer stations (0.73), Sile and Kadikoy stations (0.73), and Kilyos and Florya stations (0.72). Relatively higher correlations occurred between stations located at almost the same latitudes, both in the northern and southern parts of the city, while stations located farthest from each other both latitudinally and longitudinally exhibited lower correlation values (e.g., correlation between Sile and Florya stations—0.62). The highest correlation values among stations located in the southern part of the city were as expected, as discussed in previous sections. On the other hand, the correlation between Sile and Kilyos stations, located in the northernmost part of the city but not as close to each other as the southern stations, was relatively lower (0.70) (Figure 8a). Additionally, similar results were presented in the anomaly analyses conducted based on precipitation totals in

the previous section for the Kilyos and Sariyer stations, where the second-highest correlation was observed. Inter-station correlations in the cold season were higher compared to the warm season (Figure 8b,c). Correlation values between Florya and Kadikoy stations were notably high (0.89) during the cold season (Figure 8b). One of the main reasons for the difference in inter-station correlation values between the warm and cold seasons is believed to be the influence of convective rainfall observed during the warm season. Due to the nature of convective rainfall, its effects are often limited in scope, leading to differences in rainfall between stations.



**Figure 8.** The correlation matrices and dendrograms between stations for (a) annual, (b) cold-season, and (c) warm-season categories.

### 7. Trend Analyses of Precipitation Intensity Categories and Extreme Precipitation Indices

In this section, trend analyses were conducted first for precipitation-intensity categories, and then for extreme precipitation indices. Trend analyses help to identify whether there is an increase or decrease in the values of a random variable over time. As a result of the analyses conducted using non-parametric trend tests, at a 95% confidence level, positive trends were detected for the “light” category at three stations, while negative trends were observed for the “moderate” category at three stations as well (Table 2). It is understood that both the positive and negative trends identified are strong trends considering other parameters. No statistically significant trend was found for other variables. The positive trends observed in the “light” category at the Kilyos, Kadikoy, and Sile stations reveal a negative trend in terms of increasing rainfall intensity for these stations (Table 2).

**Table 2.** Annual trend analyses of precipitation intensity categories for each station. Green background means positive trend and red one means negative trend.

Station	Trend Test	Parameter	Light	Moderate	Heavy	Extreme
Florya	MK	P	0.99	0.01	0.85	0.55
		S	5	−707	52	−165
		Z	0.02	−2.59	0.19	−0.6
		T	0	−0.19	0.01	−0.05
	SS	Slope	0	−0.1	0	0
MK & SS		Trend (+/−/0)	(o)	(−)	(o)	(o)
Kilyos	MK	P	0.02	0.27	0.98	0.47
		S	502	232	−6	−152
		Z	2.39	1.1	−0.02	−0.72
		T	0.2	0.09	0	−0.06
	SS	Slope	0.09	0.05	0	0
MK & SS		Trend (+/−/0)	(+)	(o)	(o)	(o)
Sariyer	MK	P	0.99	0.96	0.31	0.22
		S	4	12	219	263
		Z	0.01	0.05	1.02	1.23
		T	0.2	0.01	0.08	0.1
	SS	Slope	0	0	0.03	0.02
MK & SS		Trend (+/−/0)	(o)	(o)	(o)	(o)

Table 2. Cont.

Station	Trend Test	Parameter	Light	Moderate	Heavy	Extreme
Kadikoy	MK	P	0.01	0	0.69	0.58
		S	787	−937	−127	−171
		Z	2.53	−3.01	−0.41	−0.55
		T	0	−0.21	−0.03	−0.04
	SS	Slope	0.09	−0.1	0	0
MK & SS	Trend (+/−/o)	(+)	(−)	(o)	(o)	
Sile	MK	P	0.01	0.02	0.43	0.28
		S	748	−621	210	285
		Z	2.84	−2.36	0.8	1.08
		T	0.21	−0.18	0.06	0.08
	SS	Slope	0.17	−0.11	0.01	0.02
MK & SS	Trend (+/−/o)	(+)	(−)	(o)	(o)	

As a result of the analyses conducted for eight different extreme climate indices using non-parametric trend tests, at a 95% confidence level, positive and negative trends were identified only for the Kilyos, Sariyer, and Kadikoy stations (Table 3). Regarding annual total precipitation (PRCPTOT), a positive trend was detected only at the Sariyer station. Positive trends were identified for “Rx1day” at the Kilyos and Sariyer stations; a negative trend was observed for “Rx5day” at the Kadikoy station; a positive trend was found for “R20mm” at the Sariyer station; and a negative trend was detected for “R50mm” at the Kilyos station. CDD stands for consecutive dry days, reflecting periods without significant precipitation, while CWD stands for consecutive wet days, marking periods with significant precipitation. Due to the considerable variability observed over the years, no discernible trend was identified in either index.

Table 3. Annual trend analyses of extreme climate indices for each station. Green background means positive trend and red one means negative trend.

Station	Trend Test	Parameter	PRCPTOT	Rx1 Day	Rx5 Day	R10 mm	R20 mm	R50 mm	CDD	CWD
Florya	MK	p	0.45	0.38	0.22	0.85	0.51	0.78	1	0.7
		S	−202	−232	−328	−50	−171	−64	−1	102
		Z	−0.76	−0.88	−1.24	−0.19	−0.65	−0.29	0	0.39
		τ	−0.06	−0.07	−0.09	−0.01	−0.05	−0.03	0	0.03
	SS	Slope	−0.4	−0.05	−0.14	0	0	0	0	0
MK & SS	Trend (+/−/o)	(o)	(o)	(o)	(o)	(o)	(o)	(o)	(o)	
Kilyos	MK	p	0.34	0.03	0.07	0.63	0.74	0.5	0.84	0.94
		S	196	445	369	100	−70	130	−43	−17
		Z	0.95	2.16	1.79	0.48	−0.34	0.68	−0.2	−0.1
		τ	0.08	0.17	0.14	0.04	−0.03	0.06	−0.02	−0
	SS	Slope	0.77	0.21	0.32	0	0	0	0	0
MK & SS	Trend (+/−/o)	(o)	(+)	(o)	(o)	(o)	(o)	(o)	(o)	
Sariyer	MK	p	0.01	0.05	0.2	0.09	0.05	0.03	0.21	0.2
		S	545	401	268	354	416	434	−270	274
		Z	2.59	1.91	1.27	1.69	1.99	2.2	−1.26	1.29
		τ	0.21	0.15	0.1	0.14	0.17	0.2	−0.1	0.11
	SS	Slope	2.41	0.21	0.2	0.05	0.03	0	−0.07	0
MK & SS	Trend (+/−/o)	(+)	(+)	(o)	(o)	(+)	(o)	(o)	(o)	
Kadikoy	MK	p	0.32	0.14	0.01	0.57	0.81	0.59	0.81	0.6
		S	−310	−459	−772	−179	−76	−146	76	−156
		Z	−0.99	−1.47	−2.48	−0.57	−0.24	−0.55	0.24	−0.5
		τ	−0.07	−0.1	−0.17	−0.04	−0.02	−0.05	0.02	−0
	SS	Slope	−0.51	−0.08	−0.24	0	0	0	0	0
MK & SS	Trend (+/−/o)	(o)	(o)	(−)	(o)	(o)	(o)	(o)	(o)	

Table 3. Cont.

Station	Trend Test	Parameter	PRCPTOT	Rx1 Day	Rx5 Day	R10 mm	R20 mm	R50 mm	CDD	CWD
Sile	MK	p	0.2	0.88	0.7	0.08	0.23	0.61	0.31	0.23
		S	332	−38	100	453	311	−126	−260	309
		Z	1.28	−0.14	0.38	1.75	1.2	−0.52	−1	1.21
		τ	0.1	−0.01	0.03	0.13	0.09	−0.04	−0.08	0.1
	SS	Slope	1.13	−0.01	0.05	0.05	0.02	0	−0.04	0
MK & SS	Trend (+/−/o)	(o)	(o)	(o)	(o)	(o)	(o)	(o)	(o)	

### 8. Discussion and Conclusions

This study aims to highlight the complexity of representability for rainfall, one of the most significant meteorological parameters, in complex topographic regions, and to emphasize that station-based analyses would yield more accurate results. Istanbul is an exceptional city with land on two different continents and a unique strait (the Bosphorus) connecting two seas. The city has coastal areas on both the Marmara Sea and the Black Sea on each continent. Additionally, the terrain of the city, known for its seven hills, rises from the southern to the northern parts, presenting a generally uneven landscape. The European parts of the city are generally lower and flatter, whereas the Asian parts tend to be relatively more rugged and elevated. Due to these factors, analyses were conducted by selecting two stations in the north and south of the city on both continents, along with an additional station located on the strait, to elucidate the rainfall climatology of the city.

In terms of annual total precipitation amounts, higher values were observed at three stations located in the north (Sile, Sariyer, and Kilyos) compared to stations in the south (Kadikoy and Florya). This situation is related to the city’s general exposure to northerly flows, with systems carrying moisture from the Black Sea depositing more precipitation in the northern regions. In their study examining atmospheric circulation types and their effects on precipitation in the Marmara Region, including Istanbul, Baltaci et al. (2014) found that northeasterly and easterly flow types were most frequent on an annual basis and particularly during the winter season, leading to precipitation occurrences [74]. Consequently, it was determined that northeasterly and easterly flows contribute the most to the regional average rainfall amount, and the Marmara Region generally receives significant precipitation from the northern and eastern regions, indicating the significant influence of the Black Sea on the precipitation regime in the region. It was also revealed that as one moves away from the Black Sea, precipitation at stations occurs with southerly flows. Considering the complex topography of the region, the necessity of conducting separate analyses for each station has once again been highlighted in this study. In many studies related to precipitation in the region, it has been shown that sea-effect snowfall is important for Istanbul in terms of snowfall amount, and bands of snow coming from the north over the Black Sea contribute to winter precipitation [32–38], and northerly flows are also emphasized to be important for stations located in the central and northern parts of the region during summer and spring rains [72,74,75].

Not only in terms of precipitation amounts but also in terms of the number of wet days, differences among stations have emerged. While the annual number of wet days at stations located in the north of the city varies between 112.7 days/year and 128.64 days/year, in southern stations, it has been observed to range between 103.50 days/year and 108.21 days/year. A significant difference of up to 25.14 days/year in the annual number of wet days has been identified between two different stations within the same city. It should also be noted that since most precipitation types are predominantly in the form of rain at each station, the limited impact of snowfall, ranging from 9.64 days/year to 10.65 days/year, should not be overlooked. A study conducted by Baltaci et al. (2017) stated that especially northeasterly flows lead to maximum daily rainfall potential in the Marmara Region [73]. Baltaci et al. (2012), in their study on the Marmara Region, analyzed synoptic weather types and revealed the influence of

six significant synoptic weather types in the region. According to the study results, although there are differences in proportions in both the warm and cold seasons, northerly flow types are observed at least twice as much as southerly flows [72].

Several factors have contributed to the emergence of a higher number of wet days and greater annual total precipitation amounts in the cold season compared to the warm season. Firstly, the cold season lasts longer than the warm season (7 months cold, 5 months warm). Additionally, during the cold season, the temperature gradient between cold air at higher altitudes and milder air at lower elevations is relatively stronger. This condition increases atmospheric instability and the likelihood of precipitation. Similarly, in cold weather, water vapor can condense more easily into precipitation, and the quicker condensation of water vapor creates favorable conditions for rainfall. In station-based analyses, as expected, the lowest frequency in precipitation intensity categories is observed in the “extreme” category. Extreme rainfall events are generally more frequent during the warm season [76]. Despite the relatively shorter duration of the warm season compared to the cold season, a higher frequency of “extreme” events is observed in all stations during the cold season. The primary reason for this is that the thunderstorms, both single and multicellular, which are responsible for extreme rainfall, are typically more active during this season. Thunderstorms generally result in rapid and intense rainfall. However, to determine their intensities and coverage areas, their types need to be identified. Umakanth et al. (2021) conducted statistical and dynamic analyses of thunderstorms in India, using daily rainfall totals to identify and characterize thunderstorms [77]. Hence, thunderstorms can be recognized by the amount of rainfall they produce. On the other hand, Wapler (2021) investigated mesocyclonic and non-mesocyclonic convective storms, noting that mesocyclonic storms grow and develop faster during the same time frame [78]. This underscores the significance of thunderstorm type in terms of rainfall. In the presence of multicellular thunderstorms, the system will cover a larger area and have a longer-lasting impact compared to single-cell thunderstorms. In such cases, differences in rainfall amounts between stations can occur. For example, in a single-cell thunderstorm structure, one station (Sariyer and Kilyos) may experience significant rainfall in a short period, while the other station may not. Conversely, in a multicellular structure, both stations may receive substantial rainfall. In conclusion, extreme rainfall events need to be comprehensively examined both on a station basis and regional level.

In terms of annual precipitation anomalies, the increasing frequency of positive anomaly values until the 2000s, followed by a reversal towards negative anomalies from the 2000s onwards, is an important aspect to be considered in the context of regional climate change. High correlation values between northern and southern stations were expected in terms of inter-station correlations. On the other hand, significant differences were observed in correlations between stations during the cold season compared to the warm season. The high inter-station correlations during the cold season can mostly be explained by the dominance of synoptic-scale systems. Conversely, during the warm season, the greater effectiveness of convective rainfall serves as a significant factor in the occurrence of substantial differences in rainfall between stations.

Trend analyses were conducted for both precipitation intensity categories and extreme precipitation indices associated with five different stations, but trends were mostly not detected. The most significant aspect in terms of precipitation intensity categories was the increasing trend of the “light” category at three stations, while the “moderate” category showed a decreasing trend at three stations. Positive trends in precipitation-based extreme indices were observed at the Sariyer station. Overall, satisfactory results regarding trends were not obtained in both types of analyses.

**Author Contributions:** Conceptualization: Y.K., V.Y. and C.T.; Methodology: Y.K., V.Y. and C.T.; Validation: Y.K. and V.Y.; Formal analysis: C.T.; Resources: Y.K.; Writing—original draft: Y.K. and V.Y.; Writing—review & editing: A.R.L.; Supervision: A.R.L. All authors have read and agreed to the published version of the manuscript.

**Funding:** This research received no external funding.

**Institutional Review Board Statement:** Not applicable.

**Informed Consent Statement:** Not applicable.

**Data Availability Statement:** The data presented in this study are available on request from the corresponding author. The data are not publicly available due to the data are licensed from Turkish State Meteorological Service (TSMS) in scope of this study.

**Acknowledgments:** The authors thank to Turkish State Meteorological Service (TSMS) for the data used in this study.

**Conflicts of Interest:** We hereby declare that we have no competing interests to disclose in relation to the manuscript. We have no financial, personal, or professional affiliations or relationships that could potentially influence or bias the content or findings presented in this manuscript.

## References

- Hou, A.Y.; Kakar, R.K.; Neeck, S.; Azarbarzin, A.A.; Kummerow, C.D.; Kojima, M.; Oki, R.; Nakamura, K.; Iguchi, T. The global precipitation measurement mission. *Bull. Am. Meteorol. Soc.* **2014**, *95*, 701–722. [\[CrossRef\]](#)
- Zhang, Y.; Wang, K. Global precipitation system scale increased from 2001 to 2020. *J. Hydrol.* **2023**, *616*, 128768. [\[CrossRef\]](#)
- Mondal, A.; Lakshmi, V.; Hashemi, H. Intercomparison of trend analysis of Multisatellite Monthly Precipitation Products and Gauge Measurements for River Basins of India. *J. Hydrol.* **2018**, *565*, 779–790. [\[CrossRef\]](#)
- Parker, J.K.; McIntyre, D.; Noble, R.T. Characterizing fecal contamination in stormwater runoff in coastal North Carolina, USA. *Water Res.* **2010**, *44*, 4186–4194. [\[CrossRef\]](#)
- Houze, R.A., Jr.; Rasmussen, K.L.; Medina, S.; Brodzik, S.R.; Romatschke, U. Anomalous atmospheric events leading to the summer 2010 floods in Pakistan. *Bull. Am. Meteorol. Soc.* **2011**, *92*, 291–298. [\[CrossRef\]](#)
- Sun, Q.; Miao, C.; Duan, Q.; Wang, Y. Temperature and precipitation changes over the Loess Plateau between 1961 and 2011, based on high-density gauge observations. *Glob. Planet. Chang.* **2015**, *132*, 1–10. [\[CrossRef\]](#)
- Moazami, S.; Golian, S.; Hong, Y.; Sheng, C.; Kavianpour, M.R. Comprehensive evaluation of four high-resolution satellite precipitation products under diverse climate conditions in Iran. *Hydrol. Sci. J.* **2016**, *61*, 420–440. [\[CrossRef\]](#)
- Berardy, A.; Chester, M.V. Climate change vulnerability in the food, energy, and water nexus: Concerns for agricultural production in Arizona and its urban export supply. *Environ. Res. Lett.* **2017**, *12*, 35004. [\[CrossRef\]](#)
- Papalexiou, S.M.; Montanari, A. Global and regional increase of precipitation extremes under global warming. *Water Resour. Res.* **2019**, *55*, 4901–4914. [\[CrossRef\]](#)
- Yang, T.; Li, Q.; Chen, X.; De Maeyer, P.; Yan, X.; Liu, Y.; Zhao, T.; Li, L. Spatiotemporal variability of the precipitation concentration and diversity in Central Asia. *Atmos. Res.* **2020**, *241*, 104954. [\[CrossRef\]](#)
- Ma, Q.; Lei, H.; Jia, F.; Sun, S.; Yan, P.; Gu, Y.; Feng, G. Interannual variability of extreme precipitation in late summer over west China during 1961–2021. *Front. Environ. Sci.* **2023**, *11*, 1185776. [\[CrossRef\]](#)
- Seong, C.; Sridhar, V. Hydroclimatic variability and change in the Chesapeake Bay watershed. *J. Water Clim. Chang.* **2017**, *8*, 254–273. [\[CrossRef\]](#)
- Weldegerima, T.M.; Zeleke, T.T.; Birhanu, B.S.; Zaitchik, B.F.; Fetene, Z.A. Analysis of rainfall trends and its relationship with SST signals in the lake tana basin, Ethiopia. *Adv. Meteorol.* **2018**, *2018*, 5869010. [\[CrossRef\]](#)
- Wu, J.; Chen, X. Spatiotemporal trends of dryness/wetness duration and severity: The respective contribution of precipitation and temperature. *Atmos. Res.* **2019**, *216*, 176–185. [\[CrossRef\]](#)
- Jamro, S.; Dars, G.H.; Ansari, K.; Krakauer, N.Y. Spatio-Temporal Variability of Drought in Pakistan Using Standardized Precipitation Evapotranspiration Index. *Appl. Sci.* **2019**, *9*, 4588. [\[CrossRef\]](#)
- Rahman, M.S.; Islam, A.R.M.T. Are precipitation concentration and intensity changing in Bangladesh overtimes? Analysis of the possible causes of changes in precipitation systems. *Sci. Total Environ.* **2019**, *690*, 370–387. [\[CrossRef\]](#) [\[PubMed\]](#)
- Islam, A.R.M.T.; Rahman, M.S.; Khatun, R.; Hu, Z. Spatiotemporal trends in the frequency of daily rainfall in Bangladesh during 1975–2017. *Theor. Appl. Climatol.* **2020**, *141*, 869–887. [\[CrossRef\]](#)
- Mekonen, A.A.; Berlie, A.B. Spatiotemporal variability and trends of rainfall and temperature in the Northeastern Highlands of Ethiopia. *Model. Earth Syst. Environ.* **2020**, *6*, 285–300. [\[CrossRef\]](#)
- Mumo, L.; Yu, J.; Ayugi, B. Evaluation of spatiotemporal variability of rainfall over Kenya from 1979 to 2017. *J. Atm. Solar-Ter. Phys.* **2019**, *194*, 105097. [\[CrossRef\]](#)
- Min, S.K.; Zhang, X.; Zwiers, F.W.; Hegerl, G.C. Human contribution to more-intense precipitation extremes. *Nature* **2011**, *470*, 378–381. [\[CrossRef\]](#)
- Westra, S.; Alexander, L.V.; Zwiers, F.W. Global Increasing Trends in Annual Maximum Daily Precipitation. *J. Clim.* **2013**, *26*, 3904–3918. [\[CrossRef\]](#)
- Donat, M.G.; Lowry, A.L.; Alexander, L.V.; O’Gorman, P.A.; Nicola, M. Addendum: More extreme precipitation in the world’s dry and wet regions. *Nat. Clim. Chang.* **2017**, *7*, 154–158. [\[CrossRef\]](#)

23. Ren, Z.; Zhang, M.; Wang, S.; Qiang, F.; Zhu, X.; Dong, L. Changes in daily extreme precipitation events in South China from 1961 to 2011. *J. Geogr. Sci.* **2015**, *25*, 58–68. [\[CrossRef\]](#)
24. Caloiero, T.; Coscarelli, R.; Gaudio, R. Spatial and temporal variability of daily precipitation concentration in the Sardinia region (Italy). *Int. J. Climatol.* **2019**, *39*, 5006–5021. [\[CrossRef\]](#)
25. Guo, E.; Wang, Y.; Jirigala, B.; Jin, E. Spatiotemporal variations of precipitation concentration and their potential links to drought in mainland China. *J. Clean. Prod.* **2020**, *267*, 122004. [\[CrossRef\]](#)
26. Mahmoud, M.T.; Hamouda, M.A.; Mohamed, M.M. Spatiotemporal evaluation of the GPM satellite precipitation products over the United Arab Emirates. *Atmos. Res.* **2019**, *219*, 200–212. [\[CrossRef\]](#)
27. Pawar, U.; Hire, P.; Gunathilake, M.B.; Ratnayake, U. Spatiotemporal Rainfall Variability and Trends over the Mahi Basin, India. *Climate* **2023**, *11*, 163. [\[CrossRef\]](#)
28. Anderson, T.G.; Anchukaitis, K.J.; Pons, D.; Taylor, M. Multiscale trends and precipitation extremes in the Central American Midsummer Drought. *Environ. Res. Lett.* **2019**, *14*, 124016. [\[CrossRef\]](#)
29. Xiong, J.; Yong, Z.; Wang, Z.; Cheng, W.; Li, Y.; Zhang, H.; Ye, C.; Yang, Y. Spatial and Temporal Patterns of the Extreme Precipitation across the Tibetan Plateau (1986–2015). *Water* **2019**, *11*, 1453. [\[CrossRef\]](#)
30. Bhatti, A.S.; Wang, G.; Ullah, W.; Ullah, S.; Hagan, D.F.T.; Noon, I.K.; Lou, D.; Ullah, I. Trend in Extreme Precipitation Indices Based on Long Term In Situ Precipitation Records over Pakistan. *Water* **2020**, *12*, 797. [\[CrossRef\]](#)
31. Rao, G.V.; Reddy, K.V.; Srinivasan, R.; Sridhar, V.; Umamahesh, N.V.; Pratap, D. Spatio-temporal analysis of rainfall extremes in the flood-prone Nagavali and Vamsadhara Basins in eastern India. *Wea. Clim. Ext.* **2020**, *29*, 100265. [\[CrossRef\]](#)
32. Baltaci, H.; da Silva, M.C.L.; Gomes, H.B. Climatological conditions of the Black Sea-effect snowfall events in Istanbul, Turkey. *Int. J. Climatol.* **2020**, *41*, 2017–2028. [\[CrossRef\]](#)
33. Yavuz, V.; Deniz, A.; Özdemir, E.T. Analysis of a vortex causing sea-effect snowfall in the western part of the Black Sea: A case study of events that occurred on 30–31 January 2012. *Nat. Hazards* **2021**, *108*, 819–846. [\[CrossRef\]](#)
34. Yavuz, V.; Deniz, A.; Özdemir, E.T.; Kolay, O.; Karan, H. Classification and analysis of sea-effect snowbands for Danube Sea area in Black Sea. *Int. J. Climatol.* **2021**, *41*, 3139–3152. [\[CrossRef\]](#)
35. Yavuz, V.; Lupo, A.R.; Fox, N.I.; Deniz, A. Statistical characteristics of sea-effect snow events over the western Black Sea. *Theor. Appl. Climatol.* **2022**, *150*, 955–968. [\[CrossRef\]](#)
36. Yavuz, V.; Lupo, A.R.; Fox, N.I.; Deniz, A. The role of short-wave troughs on the formation and development of sea-effect snowbands in the western Black Sea. *Theor. Appl. Climatol.* **2022**, *149*, 501–510. [\[CrossRef\]](#)
37. Yavuz, V.; Lupo, A.R.; Fox, N.I.; Deniz, A. Meso-Scale Comparison of Non-Sea-Effect and Sea-Effect Snowfalls, and Development of Prediction Algorithm for Megacity Istanbul Airports in Turkey. *Atmosphere* **2022**, *13*, 657. [\[CrossRef\]](#)
38. Yavuz, V.; Lupo, A.R.; Fox, N.I.; Deniz, A. A long-term analysis of thundersnow events over the Marmara Region, Turkey. *Nat. Hazards* **2022**, *114*, 367–387. [\[CrossRef\]](#)
39. Demirtaş, M. The high-impact sea-effect snowstorm of February 2020 over the southern Black Sea. *Acta Geophys.* **2023**, *71*, 1361–1371. [\[CrossRef\]](#)
40. Demirtaş, M. The October 2011 devastating flash flood event of Antalya: Triggering mechanisms and quantitative precipitation forecasting. *Q. J. Royal Met. Soc.* **2016**, *142*, 2336–2346. [\[CrossRef\]](#)
41. Akkoyunlu, B.O.; Baltaci, H.; Tayanc, M. Atmospheric conditions of extreme precipitation events in western Turkey for the period 2006–2015. *Nat. Hazards Earth Syst. Sci.* **2019**, *19*, 107–119. [\[CrossRef\]](#)
42. Baltaci, H. Spatiotemporal variability of climate extremes in the Marmara Region (NW Turkey). *Int. J. Global Warm.* **2019**, *28*, 239–252. [\[CrossRef\]](#)
43. Türkes, M. Spatial and temporal analysis of annual rainfall variations in Turkey. *Int. J. Climatol.* **1996**, *16*, 1057–1076. [\[CrossRef\]](#)
44. Toros, H. Spatio-temporal precipitation change assessments over Turkey. *Int. J. Climatol.* **2011**, *32*, 1310–1325. [\[CrossRef\]](#)
45. Abbasnia, M.; Toros, H. Trend analysis of weather extremes across the coastal and non-coastal areas (case study: Turkey). *J. Earth Syst. Sci.* **2020**, *129*, 95. [\[CrossRef\]](#)
46. Hadi, S.J.; Tombul, M. Long-term spatiotemporal trend analysis of precipitation and temperature over Turkey. *Meteor. Appl.* **2018**, *25*, 445–455. [\[CrossRef\]](#)
47. Şen, Z.; Habib, Z. Spatial analysis of monthly precipitation in Turkey. *Theor. Appl. Climatol.* **2000**, *67*, 81–96. [\[CrossRef\]](#)
48. Kömüşçü, A.Ü.; Aksoy, M. Long-term spatio-temporal trends and periodicities in monthly and seasonal precipitation in Turkey. *Theor. Appl. Climatol.* **2023**, *151*, 1623–1649. [\[CrossRef\]](#)
49. Unal, Y.; Deniz, A.; Toros, H.; Incecik, S. Temporal and spatial patterns of precipitation variability for annual, wet, and dry seasons in Turkey. *Int. J. Climatol.* **2010**, *32*, 392–405. [\[CrossRef\]](#)
50. Yeşilirmak, E.; Atatanır, L. Spatiotemporal variability of precipitation concentration in western Turkey. *Nat. Hazards* **2016**, *81*, 687–704. [\[CrossRef\]](#)
51. Türkes, M.; Tatlı, H. Use of the spectral clustering to determine coherent precipitation regions in Turkey for the period 1929–2007. *Int. J. Climatol.* **2010**, *31*, 2055–2067. [\[CrossRef\]](#)
52. Eris, E.; Cavus, Y.; Aksoy, H.; Burgan, H.I.; Aksu, H.; Boyacioglu, H. Spatiotemporal analysis of meteorological drought over Kucuk Menderes River Basin in the Aegean Region of Turkey. *Theor. Appl. Climatol.* **2020**, *142*, 1515–1530. [\[CrossRef\]](#)
53. Aksu, H.; Cavus, Y.; Aksoy, H.; Akgul, M.A.; Turker, S.; Eris, E. Spatiotemporal analysis of drought by CHIRPS precipitation estimates. *Theor. Appl. Climatol.* **2022**, *148*, 517–529. [\[CrossRef\]](#)

54. Aksu, H.; Taflan, G.Y.; Yaldiz, S.G.; Akgül, M.A. Evaluation of IMERG for GPM satellite-based precipitation products for extreme precipitation indices over Türkiye. *Atmos. Res.* **2023**, *291*, 106826. [[CrossRef](#)]
55. Aksu, H.; Cetin, M.; Aksoy, H.; Yaldiz, S.G.; Yildirim, I.; Keklik, G. Spatial and temporal characterization of standard duration-maximum precipitation over Black Sea Region in Turkey. *Nat. Hazards* **2022**, *111*, 2379–2405. [[CrossRef](#)]
56. Aksu, H.; Akgül, M.A. Performance evaluation of CHIRPS satellite precipitation estimates over Turkey. *Theor. Appl. Climatol.* **2020**, *142*, 71–84. [[CrossRef](#)]
57. TSMS—Turkish State Meteorological Service. Turkey’s Climate. Available online: <https://mgm.gov.tr/iklim/iklim-siniflandirmalari.aspx?m=ISTANBUL> (accessed on 22 September 2023).
58. TSMS—Turkish State Meteorological Service. Station Information. Available online: <https://www.mgm.gov.tr/kurumsal/istasyonlarimiz.aspx> (accessed on 3 September 2023).
59. Breinl, K.; Baldassarre, G.; Mazzoleni, M.; Lun, D.; Vico, G. Extreme dry and wet spells face changes in their duration and timing. *Environ. Res. Lett.* **2020**, *15*, 074040. [[CrossRef](#)]
60. Zhang, C.; Zhang, Q.; Wang, Y.; Liang, X. Climatology of warm season cold vortices in East Asia: 1979–2005. *Meteorol. Atmos. Phys.* **2008**, *100*, 291–301. [[CrossRef](#)]
61. Joshi, S.; Brown, D.; Busted, P. Intensification scenarios in projected precipitation using stochastic weather generators: A case study of central Oklahoma. *Theor. Appl. Climatol.* **2021**, *144*, 1285–1296. [[CrossRef](#)]
62. Karl, T.R.; Knight, R.W.; Easterling, D.R.; Quayle, R.G. Indices of climate change for the United States. *Bull. Am. Meteorol. Soc.* **1996**, *77*, 279–292. [[CrossRef](#)]
63. Easterling, D.R.; Evans, J.L.; Groisman, P.Y.; Karl, T.R.; Kunkel, K.E.; Ambenje, P. Observed variability and trends in extreme climate events: A brief review. *Bull. Am. Meteorol. Soc.* **2000**, *81*, 417–426. [[CrossRef](#)]
64. Ma, S.; Zhou, T.; Dai, A.; Han, Z. Observed Changes in the Distributions of Daily Precipitation Frequency and Amount over China from 1960 to 2013. *J. Clim.* **2015**, *28*, 6960–6978. [[CrossRef](#)]
65. Mann, H.B. Nonparametric Tests Against Trend. *Econometrica* **1945**, *13*, 245–259. [[CrossRef](#)]
66. Kendall, M.G. *Rank Correlation Methods*, 4th ed.; Charles Griffin: London, UK, 1975.
67. Sen, P.K. Estimates of the Regression Coefficient Based on Kendall’s Tau. *J. Am. Statist. Assoc.* **1968**, *63*, 1379–1389. [[CrossRef](#)]
68. Hamed, K.H. Trend detection in hydrologic data: The Mann–Kendall trend test under the scaling hypothesis. *J. Hydrol.* **2008**, *349*, 350–363. [[CrossRef](#)]
69. Yadav, R.; Tripathi, S.K.; Pranuthi, G.; Dubey, S.K. Trend analysis by Mann-Kendall test for precipitation and temperature for thirteen districts of Uttarakhand. *J. Agrometeorol.* **2014**, *16*, 166–171.
70. Gocic, M.; Trajkovic, S. Analysis of changes in meteorological variables using Mann-Kendall and Sen’s slope estimator statistical tests in Serbia. *Glob. Planet. Chang.* **2013**, *100*, 172–182. [[CrossRef](#)]
71. WCRP—World Climate Research Programme. Expert Team on Climate Change Detection and Indices (ETCCDI). Available online: <https://www.wcrp-climate.org/etccdi> (accessed on 3 September 2023).
72. Baltacı, H.; Kindap, T.; Ünal, A.; Karaca, M. Analysis of Synoptic Weather Types and Its Influence on Precipitation in the Marmara Region (NW Turkey). In Proceedings of the EGU General Assembly Conference 2012, Vienna, Austria, 22–27 April 2012; p. 4171.
73. Baltacı, H.; Kindap, T.; Ünal, A.; Karaca, M. The influence of atmospheric circulation types on regional patterns of precipitation in Marmara (NW Turkey). *Theor. Appl. Climatol.* **2017**, *127*, 563–572. [[CrossRef](#)]
74. Baltacı, H.; Göktürk, O.M.; Kindap, T.; Ünal, A.; Karaca, M. Atmospheric circulation types in Marmara Region (NW Turkey) and their influence on precipitation. *Int. J. Climatol.* **2014**, *35*, 1810–1820. [[CrossRef](#)]
75. Akkoyunlu, B.O.; Baltacı, H.; Tayanc, M. The Climatology, precipitation types and atmospheric conditions of extreme precipitation events in western Turkey. *Nat. Hazards Earth Syst. Sci.* **2018**. Available online: <https://nhess.copernicus.org/preprints/nhess-2018-29/nhess-2018-29.pdf> (accessed on 26 February 2024).
76. Özdemir, E.T.; Deniz, A.; Sezen, İ.; Aslan, Z.; Yavuz, V. Investigation of thunderstorms over Atatürk International Airport (LTBA) Istanbul. *Mausam* **2017**, *68*, 175–180. [[CrossRef](#)]
77. Umakanth, N.; Satyanarayana, G.C.; Naveena, N.; Srinivas, D.; Rao, D.V.B. Statistical and dynamical based thunderstorm prediction over southeast India. *J. Earth Syst. Sci.* **2021**, *130*, 71. [[CrossRef](#)]
78. Wapler, K. Mesocyclonic and non-mesocyclonic convective storms in Germany: Storm characteristics and life-cycle. *Atmos. Res.* **2021**, *248*, 105186. [[CrossRef](#)]

**Disclaimer/Publisher’s Note:** The statements, opinions and data contained in all publications are solely those of the individual author(s) and contributor(s) and not of MDPI and/or the editor(s). MDPI and/or the editor(s) disclaim responsibility for any injury to people or property resulting from any ideas, methods, instructions or products referred to in the content.